JOURNAL OF PROPULSION AND POWER
Vol. 12, No. 2, March–April 1996

Unsteady Multistage Analysis Using a Loosely Coupled Blade Row Approach

Daniel J. Dorney*
Western Michigan University, Kalamazoo, Michigan 49008
Roger L. Davis†
United Technologies Research Center, East Hartford, Connecticut 06108
and
Om P. Sharma‡
Pratt and Whitney, United Technologies, East Hartford, Connecticut 06108

The flow through gas-turbine compressors and turbines is dominated by unsteady and viscous phenomena. Accurately predicting the behavior of these complex multistage flows with unsteady rotor–stator interacting Navier–Stokes analyses can require enormous computer resources. In this investigation, an alternative method for calculating the unsteadiness associated with multiple-stage turbomachinery flows is presented. The method, called the loosely coupled blade row (LCBR) technique, utilizes single-blade row simulations coupled with the appropriate unsteady boundary conditions to predict the aerodynamic interaction effects of adjacent blade rows. The LCBR approach provides an efficient alternative to fully coupled interaction analyses while maintaining comparable accuracy.

Nomenclature

a = speed of sound
P = static pressure
U = rotor velocity
u, v = x, y components of velocity
α = absolute reference frame flow angle
β = relative reference frame flow angle
η = efficiency
ρ = density

Subscripts
t = stagnation quantity, time derivative
x, y = first derivative with respect to x, y
1 = inlet quantity
2 = exit quantity

Superscripts
~ = relative frame quantity; perturbation quantity
− = average or mean value

Introduction

THE need for improved durability, reduced noise levels, and increased performance has motivated engineers to assess the effects of flow unsteadiness on the time-mean aerodynamics in axial-flow turbomachines. In particular, recent research has focused on identifying and controlling the unsteady flow mechanisms associated with the interaction between adjacent blade rows. The two principal types of such interaction are usually referred to as potential flow and wake interaction.[1] Potential flow interaction results from the variations in the velocity potential or pressure fields associated with the blades of a neighboring row and their effect upon the blades of a given row moving at a different rotational speed. This type of interaction is of serious concern when the axial spacing between adjacent blade rows is small or the flow Mach number is high. Wake interaction is the effect upon the flow through a downstream blade row of the vortical and entropic wakes shed by one or more upstream rows.

Recently, work has been initiated to develop nonlinear, time-accurate, inviscid (Euler), and viscous (Navier–Stokes) solution techniques for unsteady flows through isolated and aerodynamically coupled blade rows (see Ref. 1 for a review). For coupled systems of rotating and stationary blade rows, the relative motions between adjacent rows give rise to unsteady aerodynamic excitations that can excite blade vibrations, generate discrete-tone noise, and degrade aerodynamic efficiency. Two categories of numerical procedures have been developed for determining the effects of relative motion between adjacent blade rows. In the first category of numerical procedures, incoming wakes are specified at the inlet of isolated blade rows.[2–5] In these methods the wakes are usually assumed to be parallel, with uniform pressure and prescribed total enthalpy and/or velocity variations. In the second category of numerical analyses, both blade rows are modeled and the relative position of one blade row is varied to simulate blade motion.[6–8] The work in this article focuses on applying the first category of numerical procedure to multiple blade rows that are loosely coupled through common unsteady boundary conditions. These inter-blade-row boundary conditions are periodically updated to include the unsteady flow effects from the upstream and downstream blade rows. This numerical technique will be referred to as the loosely coupled blade row (LCBR) method. This procedure is ideally suited for coarse-grain parallel computing since all of the blade passages can be solved simultaneously. The LCBR technique also has exceptional computational efficiency because the underlying steady flow solutions need to be solved in only a single passage of each blade row.

In recent studies, unsteady inlet and exit boundary conditions were formulated and implemented into an implicit Navier–Stokes procedure.[9–11] The two-dimensional inlet and exit boundary conditions, which are based on a characteristic analysis of the inviscid (Euler) equations of motion, were de-

Presented as Paper 95-0719 at the AIAA 33rd Aerospace Sciences Meeting and Exhibit, Reno, NV, Jan. 9–12, 1995; received Feb. 13, 1995; revision received July 28, 1995; accepted for publication Aug. 15, 1995.

*Assistant Professor, Department of Mechanical and Aeronautical Engineering. Senior Member AIAA.
†Senior Principal Engineer, Computational and Design Methods. Senior Member AIAA.
‡Chief, Aerodynamics. Senior Member AIAA.

signed to be time accurate and nonreflecting. In addition, the boundary conditions were constructed to allow the analytical specification of entropic, vortical, and acoustic excitations at the inlet, and acoustic excitations at the exit of the computational domain. In this investigation, the specification of the inlet and exit excitations is generalized to allow the use of numerically calculated profiles (or experimental data) to enable the LCBR approach. Numerical results obtained with the LCBR technique are presented for flow through a turbine stage. The results are compared with the results of a fully coupled blade row (FCBR) rotor–stator analysis and with the available experimental data.

Physical and Mathematical Description

The physical model in this study considers time-dependent flow, with negligible body forces, of a calorically perfect gas through a two-dimensional cascade of turbomachinery blades. The unsteadiness in the flow is assumed to be due to one or more of the following excitations: upstream entropic, vortical, or acoustic disturbances or downstream acoustic disturbances, that carry energy towards the blade row. Entropic and vortical disturbances can be used to model the wakes from upstream blade rows and/or combustor hot streaks entering a turbine. Acoustic disturbances model the potential flow variations associated with adjacent blade rows. The unsteady excitations are prescribed functions of location x, y and time t, and are consistent with the governing fluid dynamic equations of motion.[9,10]

The field equations considered in this investigation are the time-dependent, thin-layer Navier–Stokes equations.[12] The thin-layer assumption assumes that the viscous flux terms parallel to a solid surface are negligible with respect to the viscous terms normal to the surface. Thus, for two-dimensional turbomachinery applications, the viscous terms in the direction normal to the blade surface are retained. An eddy viscosity formulation is used to model turbulent phenomena. The turbulent viscosity for the surface boundary layers is calculated using the two-layer Baldwin–Lomax algebraic turbulence model.[12]

Solution Algorithm

The implicit numerical procedure used in this study consists of a time-marching finite difference scheme.[9,10] The procedure is second-order temporally accurate and third-order spatially accurate. The inviscid fluxes are discretized according to the scheme developed by Chakravarthy and Osher,[13] whereas the viscous fluxes are discretized using standard central differences. An alternating direction, approximate–factorization technique is used to compute the time rate changes in the primary variables. In addition, Newton subiterations can be used at each global time step to increase stability and reduce linearization errors. For typical unsteady simulations, two Newton subiterations are performed at each time step. The grid topology consists of O- and H-type overlaid grids (see Fig. 1).

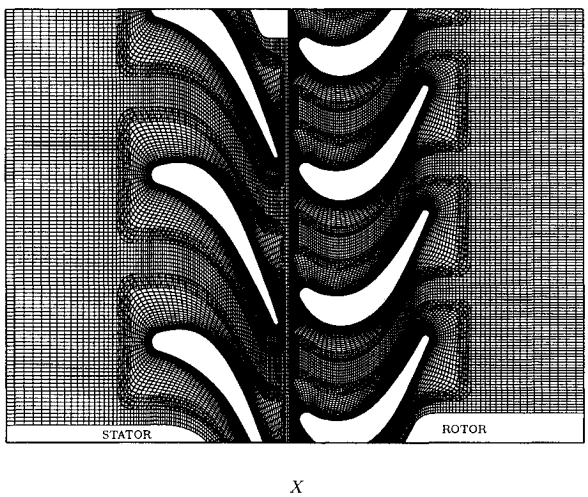

Fig. 1 Computational grids for LSRR turbine stage.

Periodic and Zonal Boundary Conditions

Periodic boundary conditions are applied in the blade-to-blade direction for H-grid and in the streamwise direction for the O-grids. The periodic boundary conditions in the computational analysis are solved implicitly using the metric information and dependent flow variables corresponding to the other side of the boundary.

The use of overlaid grids requires the application of zonal boundary conditions. Dirichlet conditions, in which the time rate change in the conserved variable vector is set to zero, are imposed at the overlaid boundaries of the O- and H-type grids. The flow variables at the zonal boundaries are explicitly updated after each time step by interpolating values from the adjacent grid. Because of the explicit application of the zonal boundary conditions, large times steps necessitate the use of more than one Newton (inner) iteration to maintain time accuracy. The accuracy of the information transfer between adjacent grids can also be enhanced by increasing the amount of overlap between the O- and H-grids. Further information describing the zonal boundary conditions can be found in Refs. 6 and 14.

Inlet, Exit, and Surface Boundary Conditions

The inlet, exit, and surface boundary conditions used in this study are based on a characteristic analysis of the linearized Euler equations. For viscous flows, it is assumed that the computational inlet and exit are in regions where the flow is predominantly inviscid, and the characteristic boundary conditions are retained. No-slip boundary conditions, along with a specified heat flux or wall temperature, are enforced at solid surfaces for viscous flows.

In the numerical analysis, quasi-two-dimensional characteristic boundary conditions are solved implicitly along with the interior of the computational domain.[9–11] After each time step, fully two-dimensional characteristic boundary conditions are explicitly applied at the inlet and exit boundaries to improve solution accuracy. This treatment, as it incorporates two-dimensional unsteady boundary conditions based on the linearized Euler equations, assumes that the convection of the wakes and propagation of acoustic waves are inviscid phenomena. Further information describing the inlet, exit, and surface boundary condition treatment can be found in Refs. 4, 9, and 11. In previous studies, the unsteady perturbations used to de-

Table 1 Timing comparison for LCBR and FCBR methods

	CPU time, min
Stator-steady	260
Stator-unsteady	540
Rotor-steady	260
Rotor-unsteady	740
Total time for LCBR method	1,800
Total time for FCBR method	25,334

Table 2 Comparison of stator inlet and exit quantities

	Steady	FCBR, time average	LCBR, time average
M_1	0.07132	0.07023	0.07005
M_2	0.19395	0.19247	0.19300
α_1	0.00 deg	0.00 deg	0.00 deg
α_2	−67.70 deg	−66.89 deg	−66.01 deg
P_2/P_1	0.9766	0.9766	0.9760

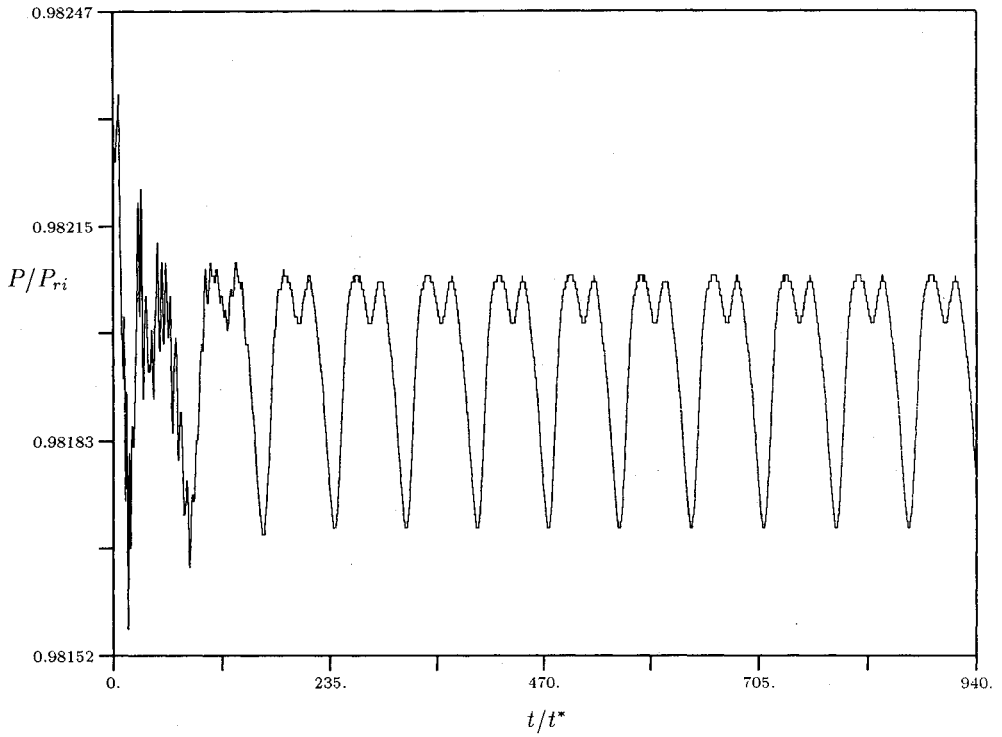

Fig. 2 Pressure history near the rotor leading edge (LCBR).

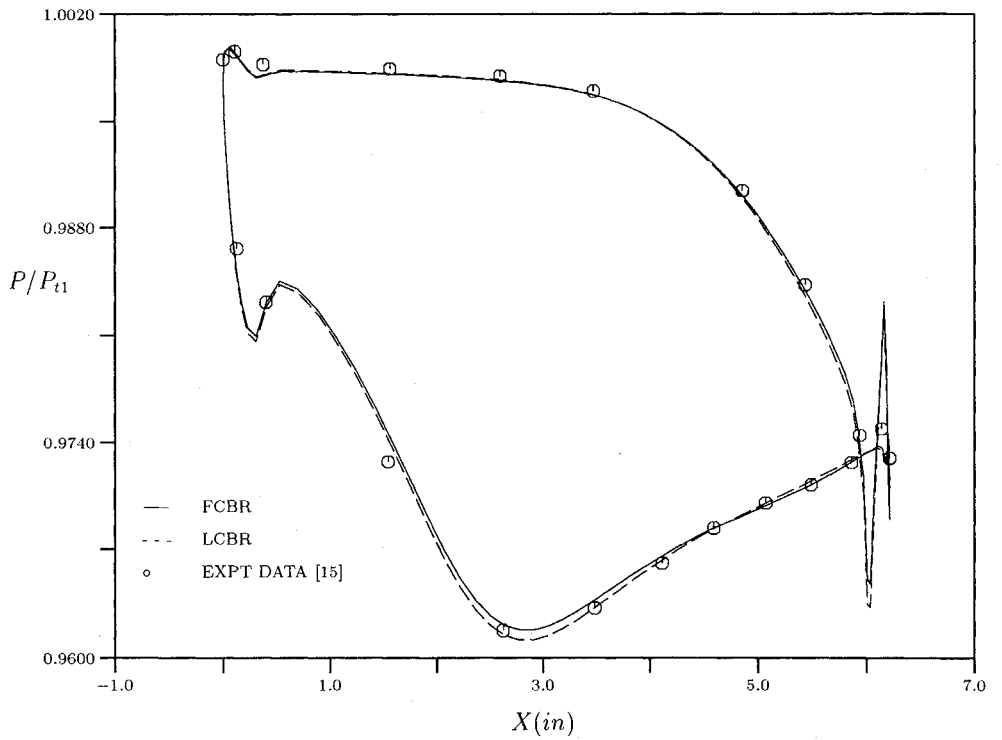

Fig. 3 Time-averaged pressure distributions for the stator.

scribe the inlet and exit excitations were based on analytical equations. In the LCBR technique, the unsteady perturbations are based on numerical simulations.

To elucidate the LCBR technique, consider the simulation of flow through a single stage (stator–rotor). The LCBR method can be applied in the following manner:

1) Steady-state solutions are obtained for both the stator and rotor blade rows. Only one blade passage needs to be solved for each blade row; the steady solutions are copied to the appropriate number of additional blade passages.

2) The exit conditions from the steady stator simulation form the basis of the unsteady inlet conditions for the rotor blade row. This is accomplished by calculating the local (scaled) perturbations of the steady stator exit quantities about the mean spatial values

$$\tilde{p}_{\text{stator}} = (p_j - \bar{p})/\bar{p} \tag{1}$$

$$\tilde{u}_{\text{stator}} = (u_j - \bar{u})/\bar{u} \tag{2}$$

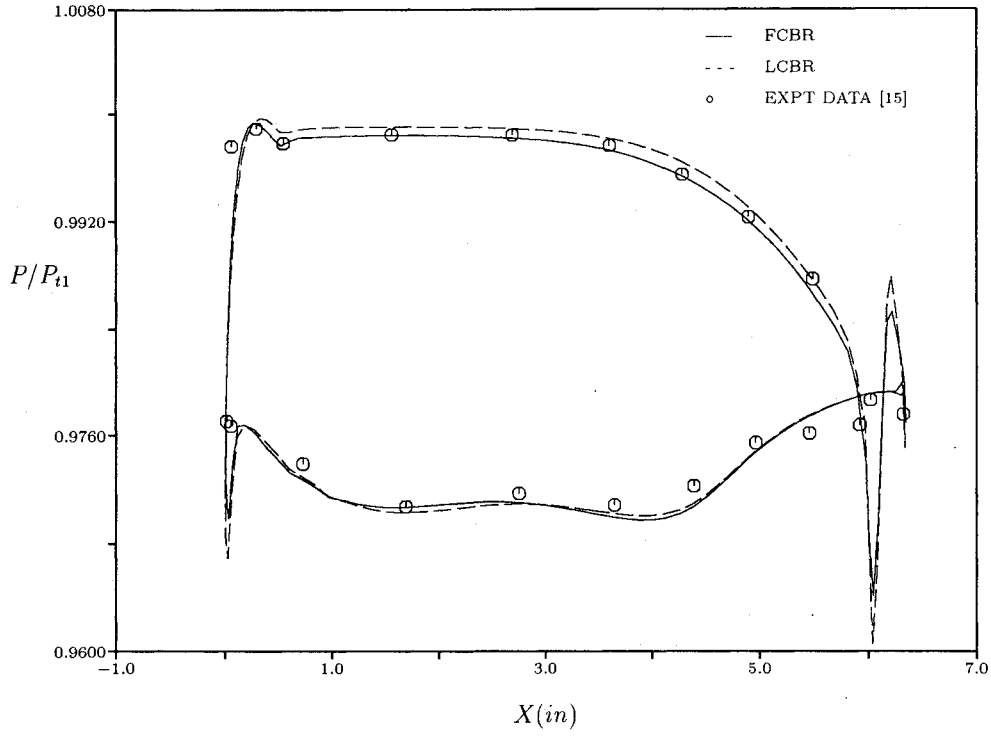

Fig. 4 Time-averaged pressure distributions for the rotor.

Table 3 Comparison of rotor inlet and exit relative reference frame quantities

	Steady	FCBR, time average	LCBR, time average
$\bar{M}_1$	0.11809	0.11641	0.11834
$\bar{M}_2$	0.16162	0.16108	0.16127
β_1	−47.27 deg	−47.66 deg	−47.84 deg
β_2	63.30 deg	63.15 deg	63.01 deg
P_2/P_1	0.9906	0.9904	0.9904
η_{stage}	0.9276	0.9252	0.9265

$$\tilde{v}_{stator} = (v_j - \bar{v})/\bar{v} \tag{3}$$

$$\tilde{P}_{stator} = (P_j - \bar{P})/\bar{P} \tag{4}$$

where the subscript stator denotes stator exit quantities. These scaled perturbations are then translated (as a function of time) in the proper direction, multiplied by the spatial mean of the rotor inlet values, and added to the spatial mean of the rotor inlet flow quantities. A steady perturbation contribution due to the difference between the steady rotor inlet flow quantities and the spatial mean of the rotor inlet quantities is also added to the sum. Since the rotor flowfield is solved in the reference frame relative to the blade, the inlet perturbations are translated in the direction opposite to the actual direction of rotor rotation. The density, for example, at the rotor inlet would be written as

$$\rho = (\bar{\rho} + \tilde{\rho})_{rotor} + (\tilde{\rho})_{stator} \tag{5}$$

where the first term in parentheses $(\bar{\rho} + \tilde{\rho})_{rotor}$ represents the steady density at the rotor inlet, and the second term in parentheses $(\tilde{\rho})_{stator}$ represents the perturbation due to the upstream blade row. The first term in parentheses is constant, while the second is a function of time and position. The characteristic variables are then formed and the unsteady boundary conditions are solved. In this manner, a simulation of the rotor passing through the stator wakes can be performed.

3) In a similar fashion, the perturbations derived from the steady rotor inlet conditions are used to form the unsteady exit conditions for the stator. For the unsteady stator simulation, the exit boundary flow perturbations are rotated in the opposite direction to that used in the unsteady rotor simulation. A simulation of the stator with an unsteady downstream pressure field can then be performed.

4) The second and third steps of this procedure can be repeated for several global interaction steps (i.e., after computing time-periodic unsteady solutions for the stator and rotor flowfields), except that the time-averaged solutions are used to calculate the new perturbation quantities. This sequence is continued until the changes in the perturbation values between two successive iterations are less than some specified small value.

Numerical Results

The geometry under consideration is the United Technologies large-scale rotating-rig (LSRR) turbine.[15] The LSRR is a large-scale, low-speed, rotating-rig, wind-tunnel facility designed to simulate the flowfield in axial-flow turbomachines. The LSRR was configured to resemble the first stage of a high-pressure turbine typical of those used in aircraft gas-turbine designs. The experimental LSRR geometry consisted of 22 stator airfoils and 28 rotor airfoils. In the present investigation, the turbine stage was modeled using three stator airfoils and four rotor airfoils. The stators were scaled down by a factor of (22/21) to maintain the pitch-to-chord ratio of the experimental configuration. A 15% axial gap was used between the stator and the rotor. The inlet Mach number to the first-stage stator was 0.07 and the inlet flow was assumed to be axial. The rotor rotational speed was 410 rpm. The freestream Reynolds number was 1×10^5/in. (39,370/cm). A pressure ratio of $P_2/P_{t1} = 0.963$ was determined from the inlet total pressure and the static pressure measured in the rotor trailing-edge plane. The airfoil surfaces were assumed to be adiabatic in the current simulations.

The computational grid topology used in the FCBR simulation is illustrated in Fig. 1. The appropriate stator and rotor portions of the FCBR grid were used in the LCBR simulations. The computational grids for the stators contained 121 × 41

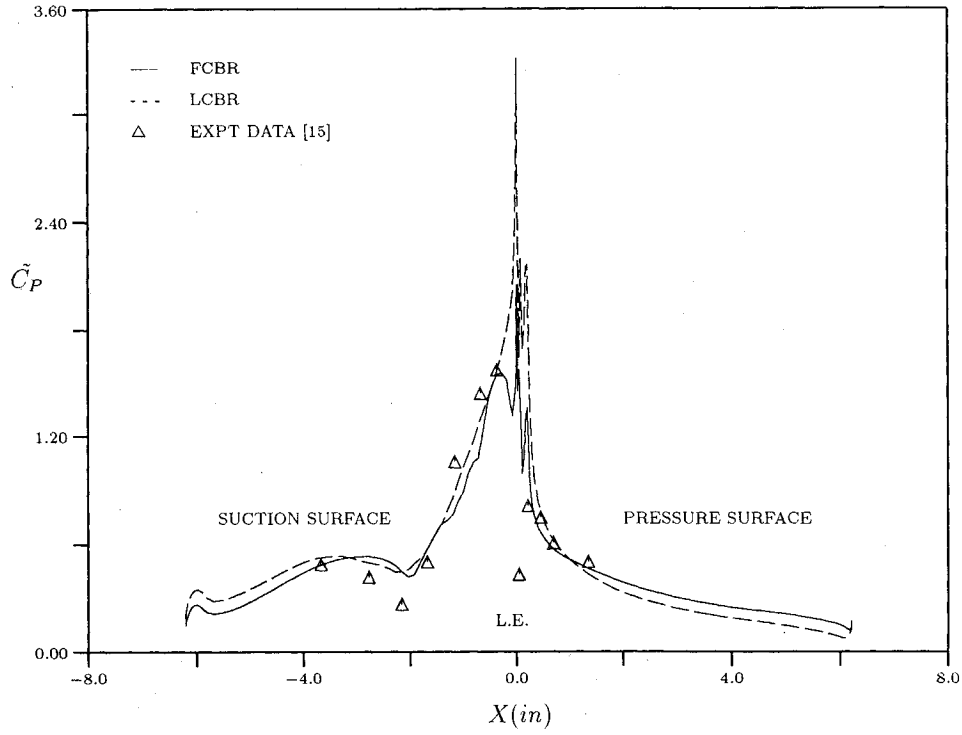

Fig. 5 Pressure amplitude coefficients for the stator.

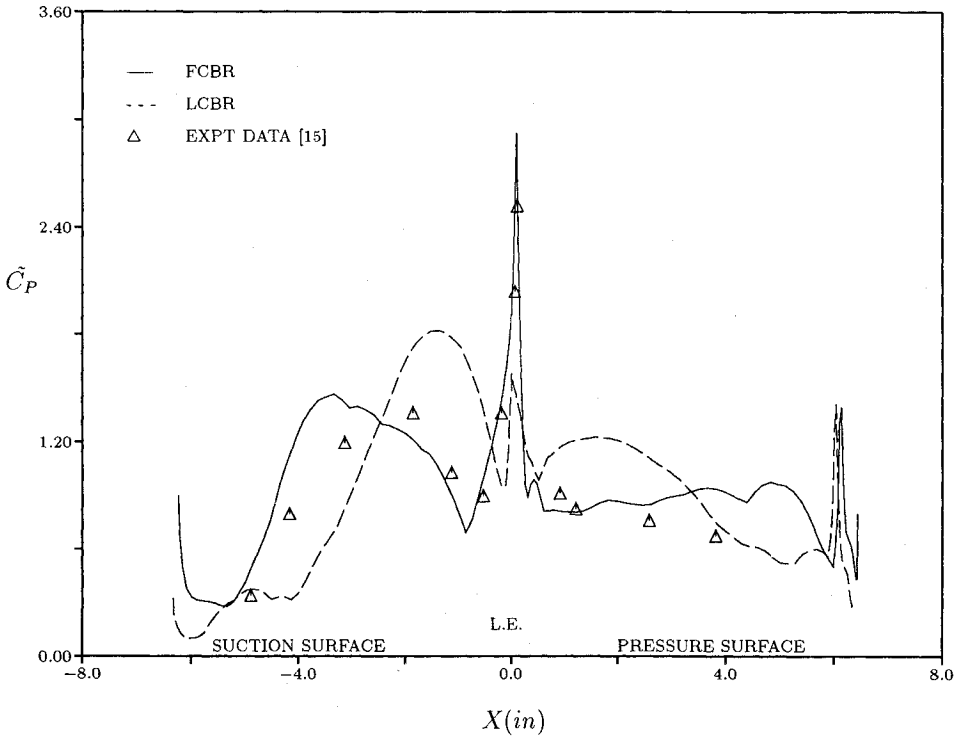

Fig. 6 Pressure amplitude coefficients for the rotor.

(streamwise × tangential) points in each O-grid and 109 × 45 points in each H-grid. The rotors were discretized using 121 × 41 points in each O-grid and 119 × 45 grid points in each H-grid. Thus, a total of 70,862 computational grid points were used in the FCBR and LCBR simulations. The final grid density was chosen to be representative of that used in a design process. The average values of y^+, the nondimensional distance of the first grid line above the wall, were 0.70 for the stator and 0.50 for the rotor, respectively. All of the computations in this investigation were performed on a Digital Equipment Corporation Alpha 3000-400 workstation.

The FCBR simulation required 10 rotor blade-passing cycles, at 4500 iterations per cycle, to attain a time-periodic solution. The LCBR approach required one global interaction iteration between the stator and rotor, with five blade-passing cycles (at 900 iterations per cycle) for each blade row during the global iteration, to achieve a time-periodic solution. Note that the LCBR approach requires the steady solution to be

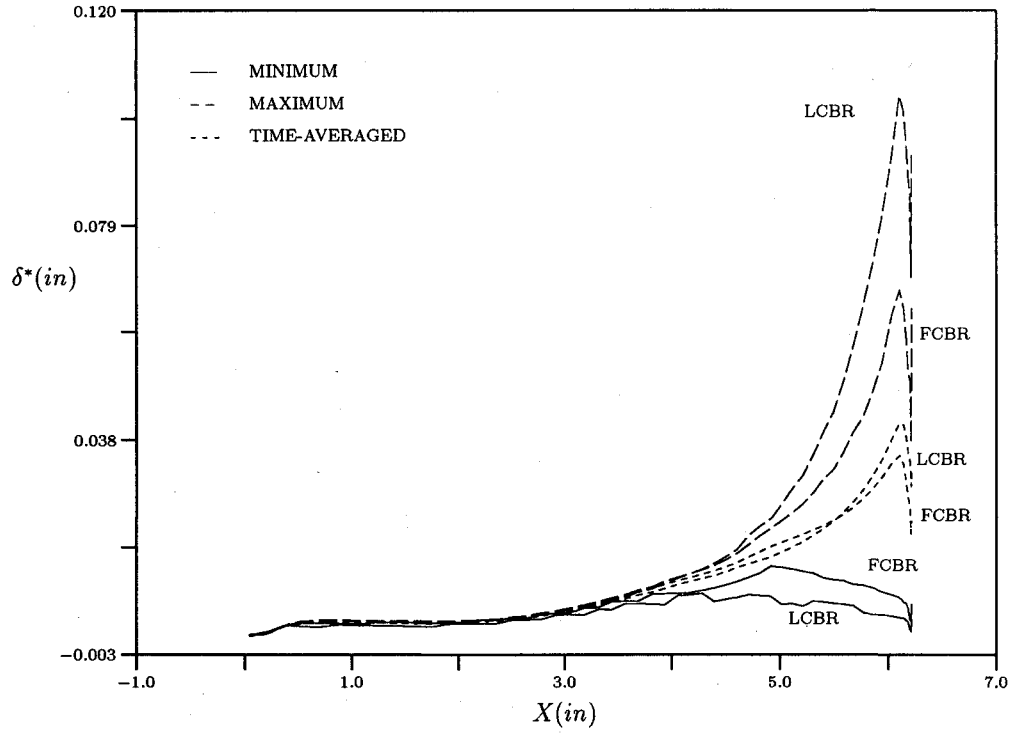

Fig. 7 Suction surface displacement thickness envelopes for the stator.

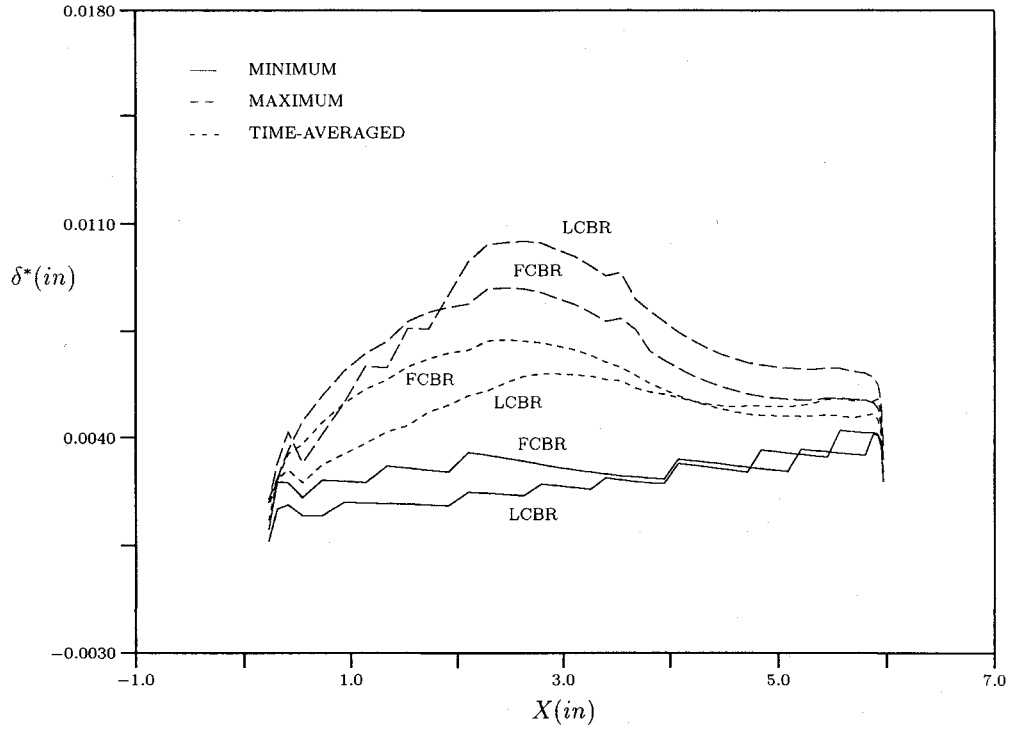

Fig. 8 Pressure surface displacement thickness envelopes for the stator.

computed in only one blade passage of the stator and rotor blade rows, respectively. Table 1 shows a comparison of the computation time required to achieve a time-periodic solution with both solution techniques. The LCBR approach required only one-fourteenth the computation time of the FCBR method. One portion of the time savings is realized by solving only one blade passage for the steady-state solutions in the LCBR procedure. Thus, the efficiency of the LCBR approach increases as the number of blade passages to be solved increases. The LCBR approach also offers a substantial reduction in computation time because the flowfield becomes time-periodic in fewer blade-passing cycles than is required with the FCBR method. Recent calculations by Chen et al.[5] have shown similar time savings by calculating unsteady solutions as perturbations to steady solutions. Figure 2 illustrates a time history of the pressure near the leading edge on the suction surface of the rotor for the LCBR simulation. The pressure in Fig. 2 has been scaled by the average static pressure at the inlet to the rotor passage. The pressure field becomes time-periodic after only a few wake-passing cycles. This suggests that the

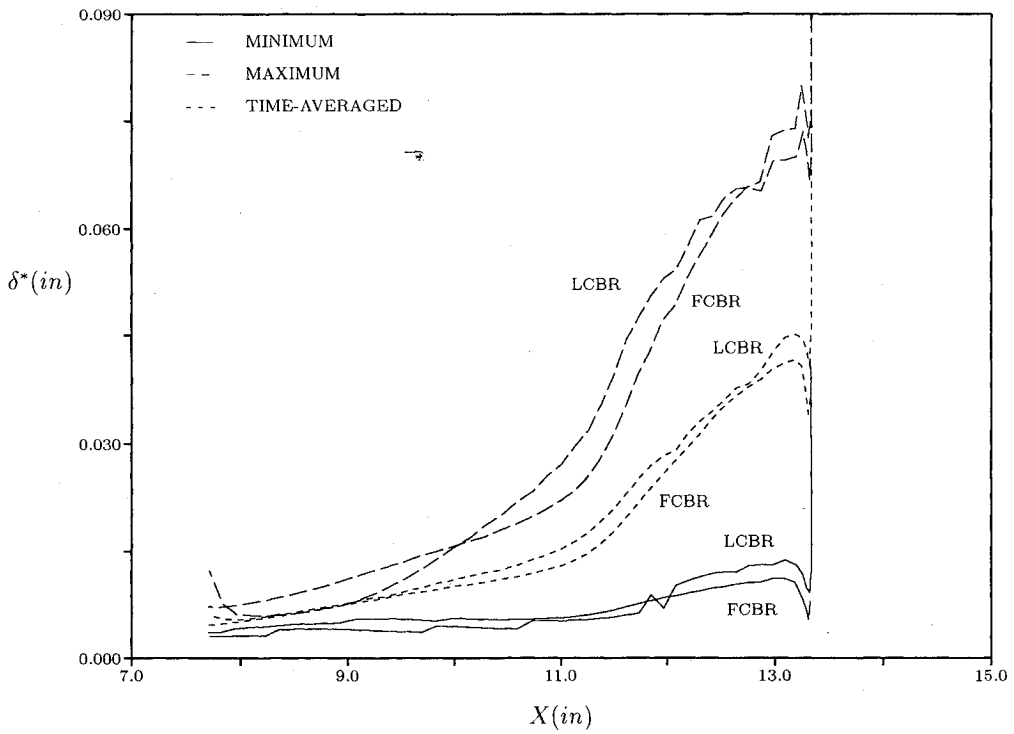

Fig. 9 Suction surface displacement thickness envelopes for the rotor.

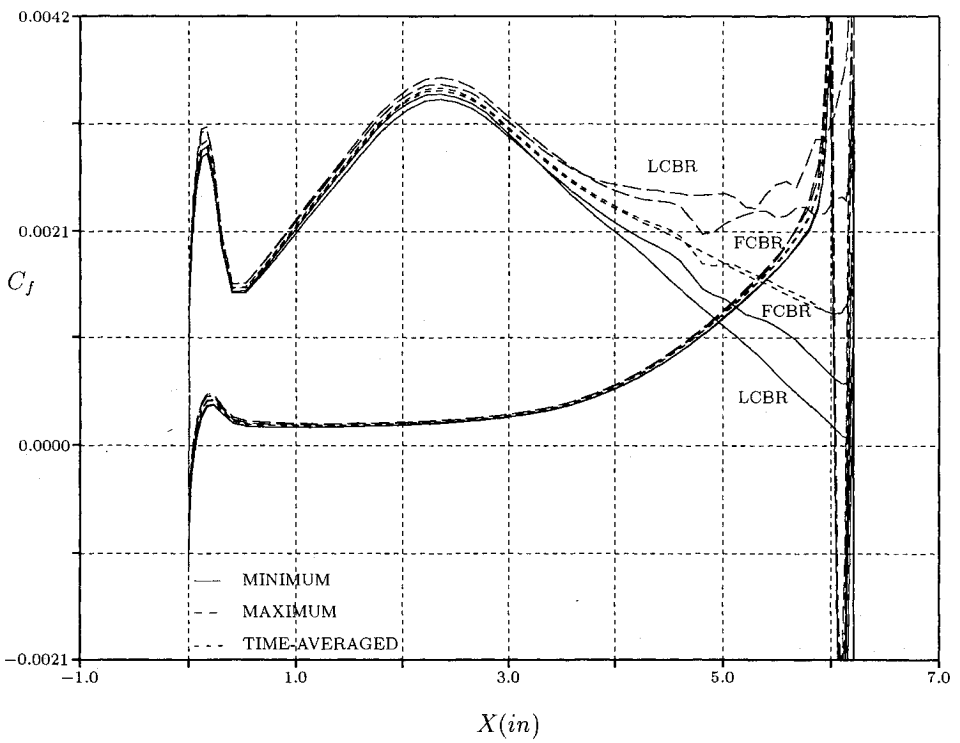

Fig. 10 Skin friction envelopes for the stator.

large number of blade-passing cycles needed to reach time-periodicity in the FCBR approach may be due to the underlying mean flow solution, and not the interaction-generated unsteadiness.

To be useful to design engineers the LCBR technique must be accurate as well as efficient. Therefore, the predicted aerodynamic and boundary-layer quantities from the LCBR and FCBR approaches have been compared. The available experimental data has been included in the comparisons.

Figure 3 illustrates the time-averaged pressure distributions for the stator obtained from the LCBR and FCBR simulations. Figure 3 also includes the experimental data of Dring et al.[15] The pressure distributions from the two simulation techniques show good agreement with each other, as well as with the experimental data. Table 2 contains the time-averaged Mach numbers, flow angles, and expansion ratio at the inlet and exit of the stator row predicted using the FCBR and LCBR techniques, as well as the results of the steady flow simulation.

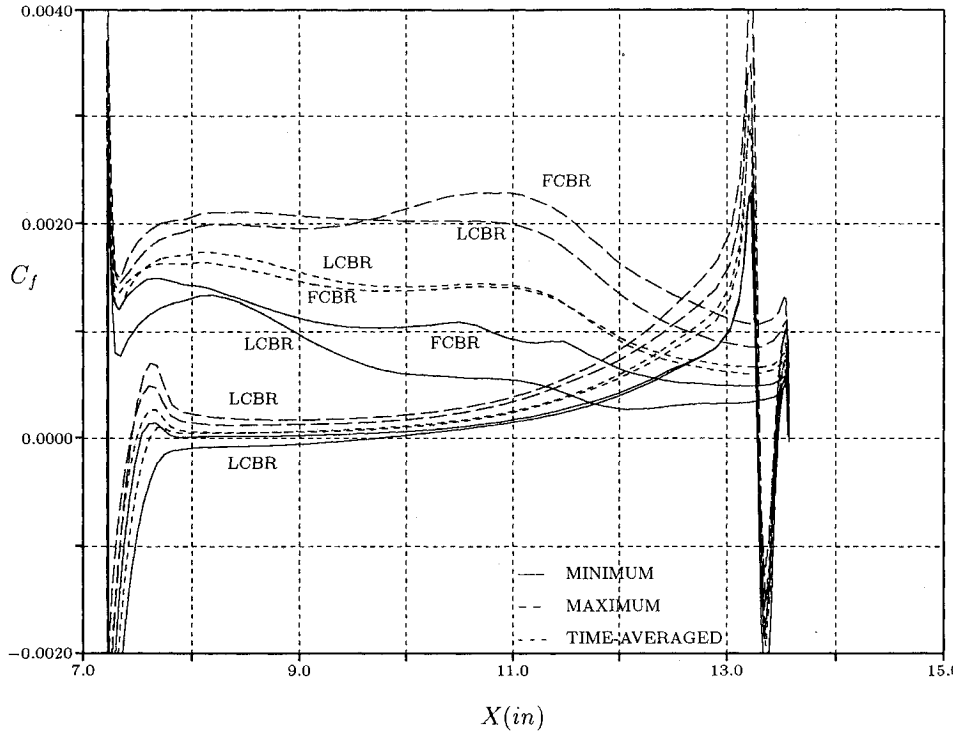

Fig. 11 Skin friction envelopes for the rotor.

The three sets of data exhibit close agreement, except for the exit flow angle. The small gap between the rotor and stator causes the exit flow angle to be affected by the trailing-edge vortex shedding.

Figure 4 contains the time-averaged pressure distributions for the rotor obtained from the LCBR and FCBR simulations. Also included in Fig. 4 is the experimental data of Dring et al. The two pressure distributions show very good agreement along the suction surface of the rotor, whereas the LCBR method predicts slightly higher pressures along the pressure surface. The results of both numerical simulations show good agreement with the experimental data. Table 3 contains the time-averaged relative reference frame Mach numbers, relative frame flow angles, and expansion ratio at the inlet and exit of the rotor row predicted using the FCBR and LCBR techniques, as well as the results of the steady flow analysis. Also included in Table 3 is the total-to-total turbine efficiencies obtained using the three solution procedures. The inlet Mach number predicted in the LCBR simulation is slightly greater than that in the FCBR simulation, but the exit Mach number and the inlet and exit flow angles compare favorably with the FCBR results. In addition, the turbine efficiency predicted using the LCBR technique shows close agreement with that predicted using the FCBR method.

A measure of the unsteadiness of the flow can be obtained by evaluating the size of the surface pressure fluctuations on the stator and rotor. The pressure fluctuations are evaluated using an unsteady pressure amplitude coefficient, which can be defined as

$$\bar{C}_p = \frac{2(P_{\max} - P_{\min})}{\rho_1 U^2} \tag{6}$$

where $P_{\min}$ represents the minimum pressure at a given location during a wake-passing cycle and $P_{\max}$ represents the maximum pressure at a given location during a wake-passing cycle. Figure 5 illustrates the unsteady pressure amplitude coefficients for the stator predicted using the LCBR and FCBR techniques as well as the experimental data.[15] The two numerical solutions are similar and display close agreement with the experimental data. Figure 6 illustrates the unsteady pressure amplitude coefficients predicted for the rotor, along with the experimental data.[15] The FCBR results show good agreement with the experimental data, although the peak in the suction surface distribution is predicted closer to the trailing edge and the pressure surface values are somewhat overpredicted near the trailing edge. The LCBR results exhibit fair agreement with the experimental data. The LCBR method underpredicts the unsteadiness near the rotor leading edge and overpredicts it along the suction and pressure surfaces. The qualitative pattern of the unsteadiness, however, is preserved with the LCBR technique.

In a recent effort, the results of the numerical flow procedure were compared with the results of a steady inviscid/viscid interaction analysis for a compressor exit guide vane and a high-speed compressor geometry.[16] In Ref. 16, the steady pressure, skin friction, and displacement thickness distributions predicted by the two analyses showed very good agreement for both test cases. In an effort to compare the unsteady viscous flowfields predicted by the FCBR and LCBR methods in the current investigation, the unsteady displacement thickness and skin friction coefficient distributions were recorded and interrogated.

Figures 7 and 8 illustrate comparisons of the suction and pressure surface displacement thickness envelopes (i.e., minimum, maximum, and time averaged), respectively, predicted using the FCBR and LCBR approaches for the turbine stator. The time-averaged distributions obtained using the two solution techniques exhibit good agreement along the suction surface of the airfoil and indicate that the displacement thickness increases from the leading edge to the trailing edge of the blade (see Fig. 7). The LCBR solution contains more unsteadiness near the trailing of the suction surface than is predicted in the FCBR simulation. Fair agreement exists between the two solutions on the pressure surface where the FCBR approach predicts larger time-averaged displacement thicknesses. Figure 9 contains the suction surface displacement thickness envelope for the turbine rotor. The two solutions exhibit very good agreement along the suction surface of the rotor. On the rotor pressure surface the edge of the boundary layer was not

well defined, and therefore, the pressure surface displacement thickness envelope is not shown.

Figure 10 illustrates a comparison of the skin friction envelopes (minimum, maximum, and time averaged) predicted for the stator. In the present investigation, the skin friction coefficient is defined as

$$C_f = 2.0\tau_w/\rho_1 V_1^2 \tag{7}$$

where τ_w is the shear stress at the blade surface and V_1 is the velocity at the stator inlet. The unsteadiness in the skin friction occurs mainly along the uncovered portion of the stator suction surface. The time-averaged distributions from the FCBR and LCBR simulations show excellent agreement over the entire blade surface, but the LCBR technique predicts more unsteadiness than that predicted in the FCBR simulation. Figure 11 shows the skin friction distributions along the rotor surface obtained using the two solution techniques. The time-averaged solutions on the suction surface show very good agreement, whereas the minimum and maximum values show fair agreement. Along the pressure surface the minimum, maximum, and time-averaged values of the two distributions show good agreement, except near the leading edge where the LCBR technique predicts a larger intermittent separation bubble.

The use of a second global coupling iteration did not significantly improve the results using the LCBR technique. Note that the specified flow angles and mass flow in the steady simulations were not adjusted to provide optimal agreement with the time-averaged FCBR simulation. In addition, the fully two-dimensional steady nonreflecting boundary conditions, which are a necessity for small rotor/stator axial gaps, allow the mass flow to float during the solution process. LCBR and FCBR simulations were also performed for an axial gap of 50%.[17] The predicted pressure, skin friction, and momentum thickness envelopes from the two techniques displayed excellent agreement.

Conclusions

An LCBR technique for multiple-blade row turbomachinery calculations has been introduced. Numerical results obtained using the LCBR technique have been compared to results from an FCBR simulation, as well as experimental data for a turbine stage. The predicted results indicate the LCBR method is more than an order of magnitude more (computationally) efficient than the FCBR approach, while maintaining acceptable accuracy. Future work will focus on improving the steady simulation technique for very small axial gaps, improving the description of the unsteady perturbations used to formulate the unsteady boundary conditions, and incorporating techniques to reduce the unsteady computation to a single passage for each blade row.

References

[1]Verdon, J. M., "Linearized Unsteady Aerodynamics for Turbomachinery Aeroelastic Applications," AIAA Paper 90-2355, July 1990.

[2]Hodson, H. P., "An Inviscid Blade-to-Blade Prediction of Wake-Generated Unsteady Flow," *Journal of Engineering for Gas Turbines and Power*, Vol. 107, April 1985, pp. 337–344.

[3]Giles, M. B., "Calculation of Unsteady Wake Rotor Interaction," *Journal of Propulsion and Power*, Vol. 4, No. 4, 1988, pp. 356–362.

[4]Giles, M. B., "Nonreflecting Boundary Conditions for Euler Equation Calculations," *AIAA Journal*, Vol. 28, No. 12, 1990, pp. 2050–2058.

[5]Chen, J. P., Celestina, M. L., and Adamczyk, J. J., "A New Procedure for Simulating Unsteady Flows Through Turbomachinery Blade Rows," American Society of Mechanical Engineers, ASME Paper 94-GT-151, June 1994.

[6]Rai, M. M., "Three-Dimensional Navier-Stokes Simulations of Turbine Rotor-Stator Interaction," *Journal of Propulsion and Power*, Vol. 5, No. 3, 1989, pp. 307–319.

[7]Rao, K. V., Delaney, R. A., and Dunn, M. G., "Vane-Blade Interaction in a Transonic Turbine Part I: Aerodynamics," *Journal of Propulsion and Power*, Vol. 10, No. 3, 1994, pp. 305–311.

[8]Rao, K. V., Delaney, R. A., and Dunn, M. G., "Vane-Blade Interaction in a Transonic Turbine Part II: Heat Transfer," *Journal of Propulsion and Power*, Vol. 10, No. 3, 1994, pp. 312–317.

[9]Dorney, D. J., "Numerical Simulations of Unsteady Flows in Turbomachines," Ph.D. Dissertation, Pennsylvania State Univ., University Park, PA, Dec. 1992.

[10]Dorney, D. J., and Verdon, J. M., "Numerical Simulations of Unsteady Cascade Flows," *Journal of Turbomachinery*, Vol. 116, No. 4, 1994, pp. 665–675.

[11]Dorney, D. J., and Davis, R. L., "Steady and Unsteady Boundary Conditions for Numerical Simulations of Flows in Turbomachines," American Society of Mechanical Engineers, ASME Paper 94-GT-152, June 1994.

[12]Baldwin, B. S., and Lomax, H., "Thin-Layer Approximation and Algebraic Model for Separated Turbulent Flows," AIAA Paper 78-257, Jan. 1978.

[13]Chakravarthy, S. R., and Osher, S., "Numerical Experiments with the Osher Upwind Scheme for the Euler Equations," AIAA Paper 82-0975, July 1982.

[14]Rai, M. M., "An Implicit, Conservative, Zonal-Boundary Scheme for Euler Equation Calculations," AIAA Paper 85-0488, Jan. 1985.

[15]Dring, R. P., Joslyn, H. D., Hardin, L. W., and Wagner, J. H., "Turbine Rotor-Stator Interaction," *Journal of Engineering for Power*, Vol. 104, Oct. 1982, pp. 729–742.

[16]Barnett, M., Verdon, J. M., and Ayer, T. C., "Development of an Efficient Analysis for High Reynolds Number Inviscid/Viscid Interaction in Cascades," AIAA Paper 92-3073, July 1992.

[17]Dorney, D. J., Davis, R. L., and Sharma, O. P., "Unsteady Multi-Stage Analysis Using a Loosely-Coupled Blade Row Approach," AIAA Paper 95-0179, Jan. 1995.